Effect of anti-solvents on the characteristics of regenerated cellulose from 1-ethyl-3-methylimidazolium acetate ionic liquid

Xiaoyan Tan, Ling Chen, Xiaoxi Li, Fengwei Xie

PII: S0141-8130(18)34044-3
DOI: https://doi.org/10.1016/j.ijbiomac.2018.11.138
Reference: BIOMAC 11015

To appear in: *International Journal of Biological Macromolecules*

Received date: 3 August 2018
Revised date: 10 November 2018
Accepted date: 14 November 2018

Please cite this article as: Xiaoyan Tan, Ling Chen, Xiaoxi Li, Fengwei Xie , Effect of anti-solvents on the characteristics of regenerated cellulose from 1-ethyl-3-methylimidazolium acetate ionic liquid. Biomac (2018), https://doi.org/10.1016/j.ijbiomac.2018.11.138

Effect of anti-solvents on the characteristics of regenerated cellulose from 1-ethyl-3-methylimidazolium acetate ionic liquid

Xiaoyan Tan [a,b,c], Ling Chen [a,*], Xiaoxi Li [a], Fengwei Xie [b,**]

[a] *Ministry of Education Engineering Research Center of Starch & Protein Processing, Guangdong Province Key Laboratory for Green Processing of Natural Products and Product Safety, School of Food Science and Engineering, South China University of Technology, Guangzhou, Guangdong 510640, China*

[b] *School of Chemical Engineering, The University of Queensland, Brisbane, Qld 4072, Australia*

[c] *College of Food Science and Light Industry, Nanjing Tech University, Nanjing, Jiangsu 211816, China*

[*] Corresponding author. Tel.: +86 20 8711 3252; fax: +86 20 8711 3252. *Email:* felchen@scut.edu.cn (L. Chen)

[**] Corresponding author. *Email:* f.xie@uq.edu.au; fwhsieh@gmail.com (F. Xie).

Abstract

This work investigates the effect of different anti-solvents (water, ethanol, or both water and ethanol) on the characteristics of cellulose dissolved and then generated from 1-ethyl-3-methylimidazolium acetate ([Emim][OAc]). Compared with original microcrystalline cellulose (MCC) granules, all regenerated celluloses showed a homogeneous, agglomerated macromorphology and had its crystalline structure transformed from original cellulose I to cellulose II. The regenerated cellulose using water (43.3%) had a higher degree of crystallinity than that using ethanol (13.5%), and a degree of crystallinity of 21.3% was obtained when an ethanol–water–ethanol treatment method was used. SAXS and FTIR results indicate that water as an anti-solvent could promote the rearrangement of cellulose molecular chains and the rebuilding of an ordered aggregated structure. Moreover, the regenerated cellulose with water showed better thermal stability than that of the samples regenerated using ethanol. Thus, our results suggest that the reconstitution of cellulose molecules during regeneration with various anti-solvents can affect the multiscale structures and properties of cellulose.

Keywords: cellulose; regeneration; anti-solvent; ionic liquid; 1-ethyl-3-methylimidazolium acetate; crystalline structure

1. Introduction

Great attention has been paid to environmentally friendly, biodegradable polymers owing to the environmental pollutions caused by excessive use of our traditional nonrenewable natural resources (coal, petroleum and gas) [1]. Cellulose, a linear polysaccharide with glucose units all linked by *β*-(1,4)-glycosidic bonds, is the most bountiful renewable biopolymer in the world [2]. Due to its attractive characteristics such as biocompatibility, biodegradability, nontoxicity, thermal and chemical stability, cellulose has been widely studied as a raw material for new "green" materials [3, 4].

To make full use of cellulose and broaden its utilization scope, the dissolution of cellulose is an important pretreatment process. However, cellulose is recalcitrant to dissolution in conventional solvents, which is mainly due to the inherent strong inter- and intra-molecular hydrogen bonding between cellulose molecular chains and its high crystallinity. Hence, it is essential to find solvents that can dissolve cellulose effectively for the utilization of cellulose. Thus far, several non-derivatizing solvent systems have been reported to dissolve cellulose, such as *N*-methylmorpholine-*N*-oxide (NMMO) [5, 6], LiCl/*N*,*N*-dimethylacetamide (DMAc) [7, 8], aqueous NaOH solution [9], and NaOH/urea system [10]. However, these systems still present some limitations because of their instability, toxicity, cost, difficulty in solvent separation, or environmental pollution [11]. These concerns need to be defeated for the environmentally friendly production of regenerated cellulose.

Ionic liquids (ILs), a kind of organic salts with a low melting point (<100 °C), have recently attracted considerable interest as a group of efficient solvents for natural biopolymers. ILs are composed of only ions and own a series of appealing characteristics such as negligible vapor pressure, outstanding solvation ability, high chemical and thermal stability, a wide temperature range to be

liquid, designability, and wide electrochemical window [12]. ILs were first claimed as "green solvents" for cellulose in 2002 [13]. Following that, extensive research has demonstrated the excellent capability of different ILs for the dissolution of cellulose, such as 1-allyl-3-methylimidazolium chloride ([Amim]Cl) [14], 1-butyl-3-methylimidazolium chloride ([Bmim]Cl) [15], and 1-ethyl-3-methylimidazolium acetate ([Emim][OAc]) [16, 17].

It is well known that regeneration is the most vital process to reconstruct or reshape dissolved cellulose into materials with desired properties. Common anti-solvents such as ethanol, water and acetonitrile perform remarkably for the regeneration of cellulose from its solutions (the separation of cellulose with its solvent). Anti-solvents are miscible with solvents but not with cellulose. Therefore, the solubility of cellulose in its solvents could be significantly reduced, leading to the precipitation of cellulose from its solutions. In recent years, the regeneration of cellulose from LiCl/DMAc solution [18], the aqueous alkali/urea system [19], 1-butyl-3-methylimidazolium acetate ([Bmim][OAc]) [20], [Bmim]Cl [21], [Amim]Cl [11] have been extensively investigated. However, there is still a lack of systematic comparison of the structures and properties between regenerated celluloses using different solvents. Moreover, the inherent mechanism of cellulose regeneration has not been fully understood.

In the present work, 1-ethyl-3-methylimidazolium acetate ([Emim][OAc]), an environmentally friendly IL, was applied to dissolve microcrystalline cellulose (MCC). After dissolution, we use different methods (only water, only ethanol, or ethanol–water–ethanol in sequence) to obtain regenerated celluloses. Then, we compared the structures and thermal properties of regenerated celluloses from the IL using different anti-solvents. Along with that, we also discussed the regeneration mechanism of cellulose from [Emim][OAc]. Our work is expected to provide important

information for the design of fabrication processes for cellulose-based materials with desired structures and properties using ILs.

2. Materials and methods

2.1 Materials

Microcrystalline cellulose (MCC) PH101, of food grade, was purchased from Linghu Xinwang Chemical Co., Ltd. (Huzhou, China); The [Emim][OAc] IL, (≥ 95% purity, *ca*. 1200 ppm water content), produced by IoLiTec Ionic Liquids Technologies GmbH (Salzstraße184, D-74076 Heilbronn, Germany), was supplied by Chem-Supply Pty Ltd (Gillman, SA, Australia). Anhydrous ethanol (analytical grade) was obtained from Merck (Darmstadt, Germany). Before use, MCC was dried at 70 °C under vacuum for 24 h, and [Emim][OAc] was kept in a vacuum oven at 90 °C for 24 h.

2.2 Dissolution and Regeneration

MCC–[Emim][OAc] homogeneous solutions (9 wt% MCC concentration) were prepared in a sealed jacketed glass vessel with magnetic stirring at 90 °C for 3 h to ensure complete dissolution. The solutions with the complete dissolution of MCC were clear and transparent and showed no birefringence crosses under a polarized light microscope (PLM).

Regenerated celluloses were obtained via a dissolution–coagulation route. Deionized water was used as an anti-solvent for precipitating cellulose from [Emim][OAc]. The MCC–[Emim][OAc] solution was poured into deionized water to obtain a coagulated cellulose hydrogel. Then, the obtained cellulose hydrogel was immersed periodically in refreshed water for 2 days at room temperature.

Similarly, regenerated celluloses were also obtained with only anhydrous ethanol or using an ethanol–water–ethanol procedure (first coagulated in ethanol, then soaked and washed in water for several times before transferred into ethanol).

The samples were dried in a vacuum oven at 40 °C and ground for further characterization. In the following discussion, the code typically as "R-MCC/W", "R-MCC/E", or "R-MCC/EWE" are used, in which "R-MCC" represents regenerated cellulose, and "W", "E", or "EWE" indicates the solvent used for regeneration, either only water, only ethanol, or ethanol–water–ethanol, respectively.

2.3 Scanning electron microscopy (SEM)

The microstructure of cellulose granules was studied using an EVO18 scanning electron microscope (Zeiss, Germany). The samples were sprinkled on a double-sided adhesive tape mounted on an aluminum specimen stub and coated with a thin layer of gold using a 108-auto sputter coater (Cressington Scientific Instruments Ltd, UK) before microscopic examination. The accelerating voltage of the SEM was 10 kV [22].

2.4 X-ray diffraction (XRD) analysis

X-ray diffraction (XRD) analysis of the samples was performed with an X'Pert PRO X-ray diffractometer (PANalytical, Netherlands) with Cu-Kα radiation at a wavelength of 0.1542 nm, operated at a voltage of 40 kV and a current of 40 mA. The scanning was detected in the diffraction angle (2θ) of 5° to 50°, with a scanning speed of 10° (2θ) per min and a scanning step of 0.033° (2θ). Each test was performed in triplicate.

Considering possible peak overlapping, PeakFit v4.12 software was used to perform peak deconvolution and evaluate the crystallinity index according to the literature [23, 24]. Specifically, the curve was smoothed by the Loess algorithm method with a level of 3%, and the parameters for the peak deconvolution were set as baseline model (linear, progressive, Tol% 5.0), peak type (spectroscopy and Gaussian Amplitude), and amplitude (10 %). The peaks of samples were divided into cellulose I crystalline peaks at around 14.8°, 16.3°, 22.6° and 34.5°, cellulose II crystalline peaks at about 12.1°, 20.1° and 21.4°, and the amorphous halo centred around 21°. The crystallinity X_c could be calculated by Eq.(1):

$$X_c(\%) = \frac{A_c}{A_c + A_a} \times 100 \qquad (1)$$

where A_c and A_a are the integrated areas of all crystalline peaks and the amorphous halo on the X-ray diffractogram, respectively.

2.5 Synchrotron small-angle X-ray scattering (SAXS) analysis

SAXS analysis of all samples was performed on the SAXS beamline (flux, 10^{13} photons per s) at the Australian Synchrotron (Clayton, Victory, Australia), with a wavelength λ = 1.47 Å. The 2D scattering patterns were collected using a Pilatus 1 M camera (active area, 169 × 179 mm; and pixel size, 172 × 172 μm) and a Pilatus 200 K camera (active area, 169 × 33 mm; and pixel size, 172 × 172 μm). The samples (*ca*. 60% MC) used for the SAXS measurement were prepared by premixing the celluloses with added water in glass vials and were equilibrated at room temperature overnight before the analysis. Each sample was placed in a 0.5 cm diameter square-like mental cell, which was sealed with two Kapton film windows and aligned perpendicular to the X-ray beam. The one-dimensional

(1D) data was obtained from the 2D scattering pattern by the scatterBrain software. The data in the angular ranges of $0.015 < q < 0.15$ Å^{-1} was used as the SAXS patterns, with $q = 4\pi \sin\theta/\lambda$ (where 2θ is the scattering angle and λ is the wavelength of the X-ray source). All the data were background-subtracted and normalized. All measurements were undertaken in triplicate.

2.6 Attenuated total reflectance Fourier-transform infrared (ATR-FTIR) spectroscopy

The ATR-FTIR spectra of samples were collected on a Nicolet 5700 FTIR spectrometer (Thermo Electron Corp, Madison, WI, USA) equipped with a Nicolet Smart Orbit ATR accessory incorporating a diamond internal reflection element. For each spectrum, 64 scans were taken in the wavenumber range of 4000–400 cm^{-1} at a resolution of 4 cm^{-1}. Each spectrum was recorded against air as the background. Three replicated measurements were recorded for each condition.

2.7 Thermogravimetric analysis (TGA)

The thermal stability of original MCC and regenerated celluloses was determined using a Mettler Toledo TGA/DSC1 thermogravimetric analyzer (Mettler-Toledo Ltd, Port Melbourne, Victoria, Australia). The samples (*ca*. 4 mg) were loaded into 70 μL alumina crucibles with a cap with a pinhole and heated from 30 °C to 750 °C at 10 °C/min under nitrogen environment. Each test was performed in triplicate.

3. Results and discussion

3.1. Granule morphology

Fig. 1 shows the SEM images of MCC and the related regenerated celluloses with different solvents. MCC displayed typical elongated and rod-like appearance with a rough and flawed surface. MCC is obtained by acid hydrolysis by partially removing its amorphous regions, which may result in the coarse surface observed here. All regenerated celluloses lost their original granule form and showed a conglomerate texture and a homogeneous macrostructure. This observation was in agreement with the results of regenerated celluloses from [Bmim][OAc] [20] and from [Bmim]Cl [13]. The agglomerates of R-MCC/W had a relatively smooth surface, while R-MCC/E showed increased surface roughness. Moreover, R-MCC/EWE displayed a degree of smoothness in the middle between R-MCC/W and R-MCC/E. The reason for the smooth surface of the regenerated cellulose coagulated in water may be due to the higher free chain mobility.

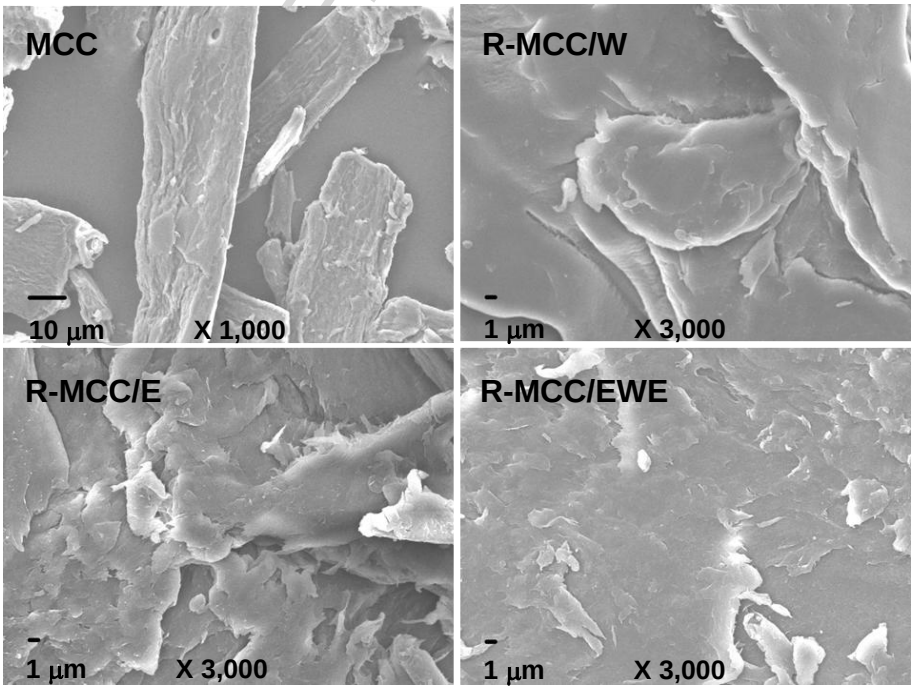

Fig. 1. SEM images of microcrystalline cellulose and regenerated celluloses with different anti-solvents.

3.2. Crystalline structure and crystallinity

Fig. 2 shows the XRD patterns of MCC and regenerated celluloses. MCC displayed main characteristic diffraction peaks at 2θ of 14.8°, 16.3°, 22.6° and 34.5°, corresponding to the crystal planes of ($1\bar{1}0$), (110), (200) and (004) with crystal spacings of cellulose I [20, 25]. All regenerated celluloses were observed to have a different diffraction pattern from that of MCC. R-MCC/W exhibited three peaks at 12.1°, 20.1°, and 21.4° 2θ, which can be assigned to the ($1\bar{1}0$), (110) and (200) lattice planes of the cellulose II crystalline structure, respectively [26]. This pattern is in agreement with that of the regenerated cellulose from [Amim]Cl [14] or [Bmim]Cl [27]. The result indicates that the reconstitution of the hydrogen-bonding network of regenerated cellulose occurred during the process of precipitation, which facilitated the formation of a cellulose II crystalline structure. Cellulose II possesses hydrogen bonds among sheets, displaying an ordered three-dimensional network [28], which makes cellulose II possess the most stable crystalline structure among all cellulose structures [29]. In contrast, the XRD pattern of the regenerated cellulose using ethanol as an anti-solvent showed a dispersive broad halo without apparent crystalline peaks, indicating a largely amorphous structure. For R-MCC/EWE, the XRD profile revealed unresolved peaks at 2θ of 20.1° and 21.4°, suggesting that a weak cellulose II crystalline structure was formed during regeneration.

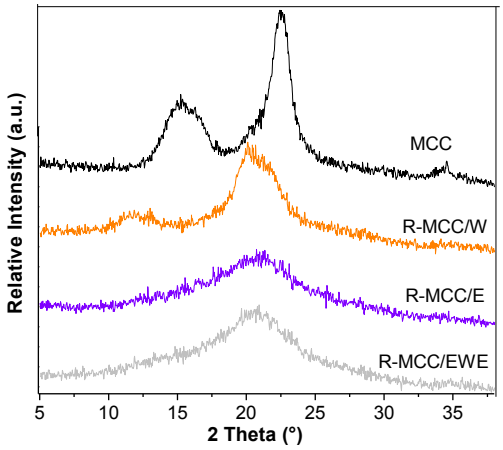

Fig. 2. XRD patterns of microcrystalline cellulose and regenerated celluloses with different anti-solvents.

The degree of crystallinity of MCC was calculated to be 56.90%, which was higher than those of regenerated celluloses. R-MCC/W, R-MCC/E and R-MCC/EWE presented degrees of crystallinity of 43.33%, 13.45% and 21.27%, respectively. Our data here suggest that R-MCC/W possessed a higher degree of crystallinity than R-MCC/E and R-MCC/EWE.

The crystallites of MCC could be completely damaged during dissolution, which was caused by the cleavage of the inter- and intra-molecular hydrogen bonds in MCC [16]. Then, by regeneration, the molecular chains of cellulose rearranged and reconstituted into an aggregated structure. Our results here reveal that water plays an important role in the reconstitution of crystallites during regeneration. When water is used for regeneration, cellulose chains have a higher tendency to realign into a rigid, ordered structure and form crystallites. This can be explained by the strong hydrogen-bonding interactions between water and the IL, which facilitates the aggregation of cellulose chains.

3.3. Nano-aggregation structure

SAXS is a potent method to understand not only the phase behaviors of polymers in condensed and solution states, but also the perturbed or nonperiodic structures of amorphous and mesomorphic materials [30, 31]. **Fig. 3** shows the double-logarithmic SAXS patterns (a) and $I^*q^2 - q$ SAXS patterns (b) of MCC and regenerated celluloses, respectively. As exhibited in **Fig. 3a**, MCC and all regenerated celluloses possessed a wide scattering peak in the q range of 0.04~0.15 $Å^{-1}$, implying that MCC contained an orderly arranged structure on the nanoscale and regenerated celluloses also had an ordered aggregated structure. Although the multiscale structures of MCC were destroyed and disorganized after dissolution in [Emim][OAc], linear cellulose molecules could aggregate and rearrange during the regeneration process, forming some ordered structure.

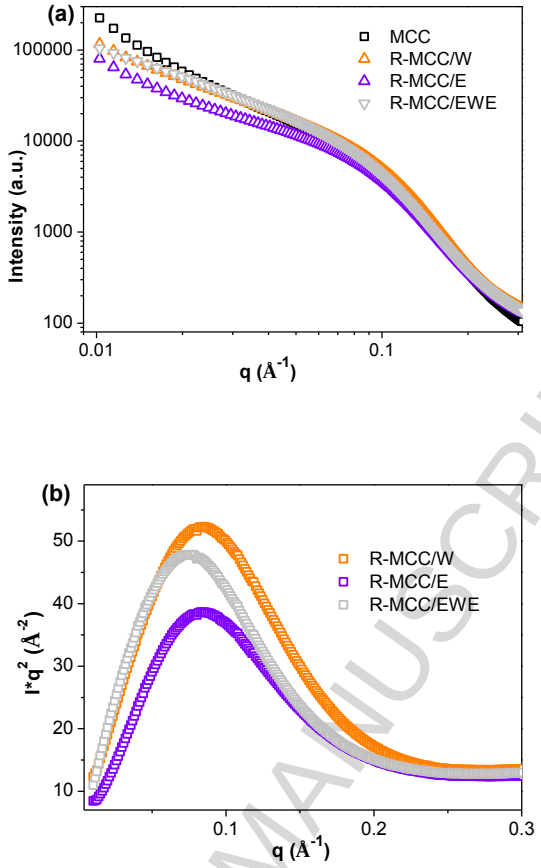

Fig. 3. Double-logarithmic SAXS patterns (a) and $I^*q^2 - q$ SAXS patterns (b) of microcrystalline cellulose and regenerated celluloses with different anti-solvents.

The aggregated structure (the ordered region and amorphous region on the nanoscale) of regenerated cellulose could be studied by SAXS. As seen in **Fig. 3b**, obvious scattering peaks in a low q range of regenerated samples were shown after the Lorentz correction [32], which should be due to the difference in electron density between the ordered and amorphous regions. The order degree of cellulose molecules could be quantified by calculating the area ($A_q = \int_0^\infty Iq^2 dq$) [33] under the curves in **Fig. 3b**. The integrated areas (A_q) for R-MCC/W, R-MCC/E and R-MCC/EWE were 4.289, 3.082, and 3.720, respectively. These data suggest that the cellulose regenerated using water possessed the

highest ordered chains, while the cellulose regenerated using ethanol had the lowest order degree of chains.

For a two-component system polymer, SAXS scattering intensity can be influenced by the electron density difference between the ordered and amorphous regions, $\Delta\rho = \rho_o - \rho_a$ (where ρ_o and ρ_a are the electron densities of the ordered and amorphous regions of the polymer, respectively) [34, 35]. It could be seen from **Fig. 3a** that the SAXS intensity of regenerated samples followed the sequence of R-MCC/W > R-MCC/EWE > R-MCC/E, indicating that the electron density difference between the ordered and amorphous regions of R-MCC/W was higher than that of R-MCC/EWE and R-MCC/E, whilst R-MCC/EWE was in the middle. This observation corresponds to the XRD results. The molecular chains of R-MCC/W were more organized with a cellulose II crystalline structure formed, as reflected by the largest ρ_o and the highest $\Delta\rho$. R-MCC/EWE showed the lower scattering intensity of its nanoaggregation, and its decreased $\Delta\rho$ might be due to the less ordered regions and the weak cellulose II crystalline structure. Although R-MCC/E rearranged into some ordered structure during regeneration, this regenerated cellulose had the lowest degree of crystallinity, which can be shown by its lowest ρ_o and $\Delta\rho$.

3.4. Molecular chain structure

ATR-FTIR measurements were conducted to analyze the changes in molecular structure in MCC and regenerated celluloses using different anti-solvents and the corresponding spectra are shown in **Fig. 4**. MCC presented a broad band in the region of 3600–3100 cm^{-1}, which can be assigned to the stretching vibration of -OH groups, indicating the inter- and intra-molecular hydrogen bonding of

cellulose chains [36]. The band in the region of 3000–2800 cm^{-1} was attributed to the C-H stretching. The prominent band at 1057 cm^{-1} could be related to the C-O-C pyranose ring skeletal vibration [37]. The FTIR spectra of R-MCC/W, R-MCC/E and R-MCC/EWE all matched the functional groups of MCC, with no new characteristic peaks emerging. Therefore, it can be concluded that the chemical structure of cellulose remained unchanged and there was no particular derivatization reaction during the course of dissolution and regeneration in [Emim][OAc]. Moreover, the characteristic FTIR absorption peaks at 1378 cm^{-1} and 1567 cm^{-1} of [Emim][OAc] [16, 38] could not be found, which proved no [Emim][OAc] remained in regenerated celluloses.

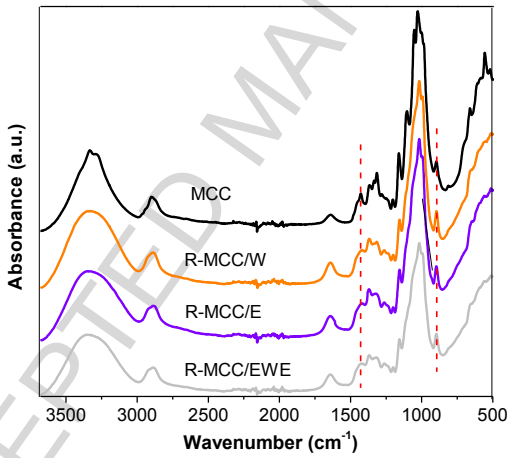

Fig. 4. FTIR spectra of microcrystalline cellulose and regenerated celluloses with different anti-solvents.

However, some differences can be found between the IR spectra of MCC and regenerated celluloses, which could be due to the variation of cellulose crystalline structure. The band at 1430 cm^{-1} corresponds to the -CH_2 symmetric bending vibration [37], and it is known as the "crystallinity band" in cellulose I [39, 40]. Compared with MCC, this absorption band of all regenerated celluloses weakened and shifted to the left, suggesting that the cellulose I structure was transformed into another

type of cellulose crystalline structure or amorphous structure after regeneration. The absorption band at 895 cm^{-1} assigned to the C-O-C asymmetric stretching at the β-(1,4)-glycosidic linkage was usually considered as an "amorphous band" in amorphous cellulose and cellulose II [41]. For all regenerated celluloses, the intensity of the amorphous band was seen to increase, which suggests the reduced crystallinity and weakened inter- and intramolecular hydrogen bonding. Regarding crystallinity, the FTIR results here were in conformity with our XRD results.

3.5. Thermal analysis

TGA analysis was carried out to study the thermal stability of MCC and regenerated celluloses. **Fig. 5** shows the weight loss curves and the derivative weight loss curves of the different samples. The related parameters were summarized in **Table 1**. All the samples experienced a small weight loss between 40 °C and 100 °C (**Fig. 5**) corresponding to the evaporation of free water from the cellulose. With the increased temperature, all the samples presented a sharp weight loss between 200 °C and 390 °C due to the depolymerization, dehydration and decomposition of cellulose [42]. As summarized in **Table 1**, the thermal degradation of MCC began at 270 °C (onset temperature, T_{onset}) and reached its maximum rate at 350 °C (peak temperature, T_{peak}). Regenerated samples were found to be less thermally stable than MCC, and the T_{onset} values of R-MCC/W, R-MCC/E and R-MCC/EWE were 215 °C, 162 °C and 204 °C respectively. The thermal degradation range of regenerated celluloses could be divided into two ranges. According to previous reports, the decomposition of polysaccharide (like cellulose or starch) occurred by scission of glycosidic linkages first and followed by pyranose ring rupture [43, 44]. Regenerated celluloses degraded in the lower range of 200–300 °C were

probably attributed to the partial molecule degradation after dissolution and regeneration in [Emim][OAc]. What's more, the hydrogen bonding network and crystal structure of cellulose were destroyed during these courses, leading to the decrease in thermal stability of regenerated celluloses. While some order structure cellulose after rearrangement still had high thermal stability and could be degraded over 300 °C. The reconstitution of polysaccharide chains during regeneration with different anti-solvents could also affect the thermal properties of cellulose. In agreement with the XRD and SAXS results, water was more instrumental in the rebuilding of a hydrogen-bonding network and an ordered structure, thus R-MCC/W and R-MCC/EWE had a relatively higher thermal stability than that of R-MCC/E.

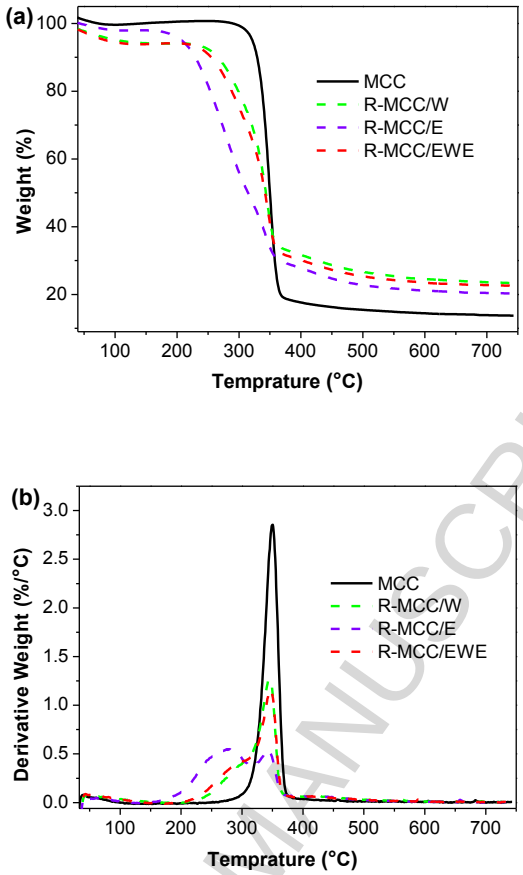

Fig. 5. Weight loss curves (a) and derivative weight loss curves (b) of microcrystalline cellulose and regenerated celluloses with different anti-solvents.

Table 1. Decomposition onset temperatures (T_{onset}) and peak decomposition temperatures (T_{peak}) of microcrystalline cellulose and regenerated celluloses

Sample	T_{onset} (°C)	T_{peak} (°C)
MCC	270	350
R-MCC/W	215	303, 343
R-MCC/E	162	276, 342
R-MCC/EWE	204	302, 347

3.6. Mechanism of cellulose regeneration in [Emim][OAc]

On the basis of the analyses discussed above, the possible mechanism regarding the regeneration of cellulose with different anti-solvents from [Emim][OAc] is proposed in **Fig. 6**. The cellulose molecular chains are associated with the strong inter- and intra-molecular hydrogen bonding, forming a stable aggregated structure with crystalline and amorphous regions. The $[OAc]^-$ anion of [Emim][OAc] has strong protonation capability, thus can interact with cellulose hydroxyls to disrupt the inherent strong hydrogen-bonding network and destruct the original aggregated structure of MCC. Owing to this, cellulose can be dissolved and its chains are dispersed homogeneously in [Emim][OAc] with heating, which can be seen in **Fig. 6a**. After that, cellulose can be regenerated from the MCC–[Emim][OAc] solution by the treatment with an anti-solvent (e.g., water or ethanol) without any derivative reaction.

When water is used as an anti-solvent, it can easily to penetrate into the MCC–[Emim][OAc] system and react with both the $[OAc]^-$ anion of [Emim][OAc] and the cellulose hydroxyl groups via hydrogen bonding, leading to easier aggregation and rearrangement of cellulose molecular chains. The cellulose hydrogel (R-MCC/W) is then obtained via the formation of physical crosslinking domains by the crystallite hydrates of cellulose II, the hydrogen bonding between cellulose molecular chains, and chain entanglements (**Fig. 6b**). When anhydrous ethanol is added into the MCC–[Emim][OAc] solution, it can also interact with the $[OAc]^-$ anion of [Emim][OAc] by hydrogen bonding, leaving the cellulose chains twined and aggregated. As shown in **Fig. 6c**, the chains can realign into ordered regions with a relatively loosened aggregated structure, but have less tendency to participate in forming cellulose crystallites in ethanol. In this way, R-MCC/E becomes a more amorphous material.

Both water and ethanol can beat solvent molecules to form hydrogen bonding to result in the cellulose regeneration from the dissolution. For one thing, the polarity of water molecule is greater than ethanol molecule, so the water is easier to form hydrogen bonding with cellulose. For another, water molecules play an important role in the formation of cellulose crystallites. Therefore, regeneration in water allows the formation of more organized and crystalline-structured cellulose. The anti-solvent during regeneration plays a crucial role in controlling the structure and properties of regenerated cellulose.

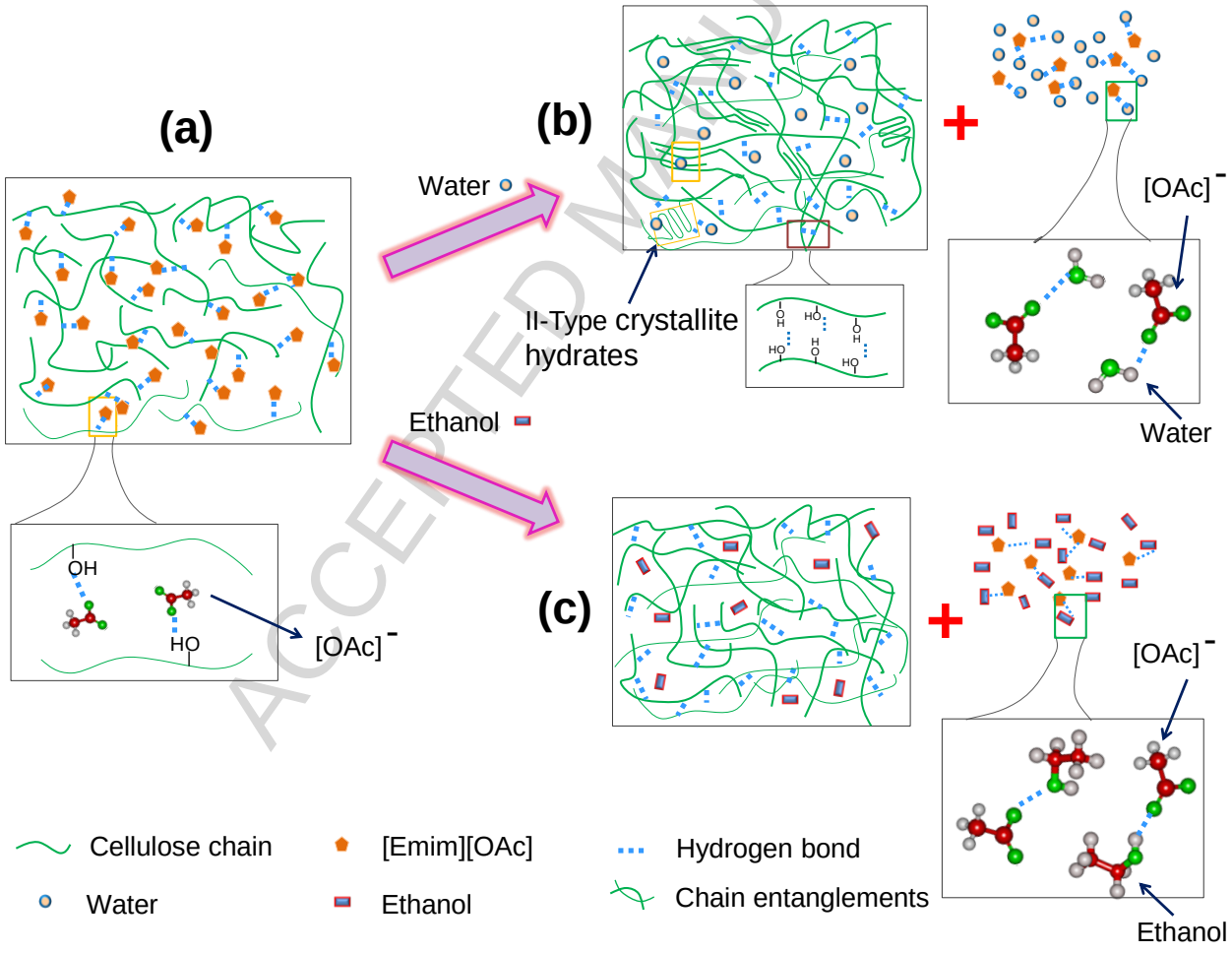

Fig. 6. Schematic representations of the regeneration of cellulose from [Emim][OAc].

4. Conclusion

In this study, we found that investigated the anti-solvent (either water, ethanol, or water–ethanol–water as an anti-solvent) plays a crucial role in controlling the structure and thermal property of cellulose during generation from [Emim][OAc]. When water was used as an anti-solvent, it could facilitate the realignment of molecular chains and the rebuilding of an ordered cellulose structure. In contrast, ethanol as an anti-solvent would force cellulose chains to aggregate into a relatively loose and disorganized state. The molecular order of regenerated celluloses was in the sequence of R-MCC/W > R-MCC/EWE > R-MCC/E. XRD analysis indicated that the cellulose I crystalline structure of MCC was transformed into a cellulose II structure after dissolution in [Emim][OAc] and regeneration. R-MCC/W, R-MCC/E and R-MCC/EWE presented degrees of crystallinity of 43.33%, 13.45% and 21.27%, respectively. This difference in the aggregated and crystalline structures of regenerated celluloses corresponds to the thermal stability of regenerated celluloses, with R-MCC/W being most thermally stable and R-MCC/E the least thermally stable. The knowledge from this work is expected to provide guidance to the design of fabrication processes of cellulose-based materials with desired structures and properties using ILs.

Acknowledgments

This work is supported by the Key Project of Guangzhou Science and Technology Program (No.201804020036), the YangFan Innovative and Entrepreneurial Research Team Project (2014YT02S029), and the Open Project Program of Provincial Key Laboratory of Green Processing Technology and Product Safety of Natural Products (KL-2018-20). Part of this research was

undertaken on the SAXS/WAXS beamline at the Australian Synchrotron, Victoria, Australia. X. Tan also would like to thank the China Scholarship Council (CSC) for the financial support for his visiting studies at The University of Queensland (UQ) as part of his PhD work.

References

[1] E. Ten, W. Vermerris, Polymers, 5 (2013) 600-642.

[2] Y.J. Oyeniyi, O.A. Itiola, International Journal of Pharmacy & Pharmaceutical Sciences, 4 (2012) 197-200.

[3] J. Sethi, M. Farooq, S. Sain, M. Sain, J.A. Sirvio, M. Illikainen, K. Oksman, Cellulose, 25 (2018) 259-268.

[4] M. Soheilmoghaddam, H. Adelnia, G. Sharifzadeh, M.U. Wahit, T.W. Wong, A.A. Yussuf, Cellulose, 24 (2017) 811-822.

[5] F. Wendler, Z. Persin, K. Stana-Kleinschek, M. Reischl, V. Ribitsch, A. Bohn, H.-P. Fink, F. Meister, Cellulose, 18 (2011) 1165-1178.

[6] H.P. Fink, P. Weigel, H.J. Purz, J. Ganster, Progress In Polymer Science, 26 (2001) 1473-1524.

[7] Y. Ono, T. Ishida, H. Soeta, T. Saito, A. Isogai, Biomacromolecules, 17 (2016) 192-199.

[8] S.L. Williamson, C.L. McCormick, Journal Of Macromolecular Science-Pure And Applied Chemistry, A35 (1998) 1915-1927.

[9] Y.N. Kuo, J. Hong, Polymers for Advanced Technologies, 16 (2005) 425-428.

[10] J. Cai, L. Zhang, Macromolecular Bioscience, 5 (2005) 539-548.

[11] K.O. Reddy, C.U. Maheswari, M.S. Dhlamini, B.M. Mothudi, J. Zhang, J. Zhang, R. Nagarajan, A.V. Rajulu, Carbohydrate Polymers, 160 (2017) 203-211.

[12] K.E. Gutowski, Physical Sciences Reviews, (2018).

[13] R.P. Swatloski, S.K. Spear, J.D. Holbrey, R.D. Rogers, Journal Of the American Chemical Society, 124 (2002) 4974-4975.

[14] H. Zhang, J. Wu, J. Zhang, J.S. He, Macromolecules, 38 (2005) 8272-8277.

[15] J. Wang, T. Wang, J. Xu, J. Yu, Y. Zhang, H. Wang, Journal Of Applied Polymer Science, 135 (2018).

[16] X. Tan, X. Li, L. Chen, F. Xie, Physical Chemistry Chemical Physics, 18 (2016) 27584-27593.

[17] M. FitzPatrick, P. Champagne, M.F. Cunningham, Carbohydrate Polymers, 87 (2012) 1124-1130.

[18] Y. Wan, F. An, P. Zhou, Y. Li, Y. Liu, C. Lu, H. Chen, Chemical Communications, 53 (2017) 3595.

[19] P. Yu, H. He, A. Dufresne, Materials Letters, 205 (2017) 202-205.

[20] Z. Liu, X. Sun, M. Hao, C. Huang, Z. Xue, T. Mu, Carbohydrate Polymers, 117 (2015) 99-105.

[21] A.P. Dadi, S. Varanasi, C.A. Schall, Biotechnology And Bioengineering, 95 (2006) 904-910.

[22] J. Chen, X. Li, L. Chen, F. Xie, Carbohydrate Polymers, 191 (2018) 242-254.

[23] C. Ruan, Y. Zhu, X. Zhou, N. Abidi, Y. Hu, J.M. Catchmark, Cellulose, 23 (2016) 3417-3427.

[24] S. Park, J.O. Baker, M.E. Himmel, P.A. Parilla, D.K. Johnson, Biotechnology for biofuels, 3 (2010) 10.

[25] G. Sebe, F. Ham-Pichavant, E. Ibarboure, A.L.C. Koffi, P. Tingaut, Biomacromolecules, 13 (2012) 570-578.

[26] Q. Lu, W. Lin, L. Tang, S. Wang, X. Chen, B. Huang, Journal Of Materials Science, 50 (2015) 611-619.

[27] J. Han, C. Zhou, A.D. French, G. Han, Q. Wu, Carbohydrate Polymers, 94 (2013) 773-781.

[28] P. Langan, Y. Nishiyama, H. Chanzy, Journal Of the American Chemical Society, 121 (1999) 9940-9946.

[29] S.H. Lee, T.V. Doherty, R.J. Linhardt, J.S. Dordick, Biotechnology And Bioengineering, 102 (2009) 1368-1376.

[30] B. Chu, B.S. Hsiao, Chemical Reviews, 101 (2001) 1727-1761.

[31] H. Wang, Y. Liu, L. Chen, X. Li, J. Wang, F. Xie, Food Chemistry, 242 (2018) 323-329.

[32] N. Stribeck, X-ray scattering of soft matter, Springer Science & Business Media, 2007.

[33] W. Situ, L. Chen, X. Wang, X. Li, Journal Of Agricultural And Food Chemistry, 62 (2014) 3599-3609.

[34] X. Li, Y. He, C. Huang, J. Zhu, A.H.-M. Lin, L. Chen, L. Li, Food Control, 66 (2016) 130-136.

[35] J. Zhu, X. Li, C. Huang, L. Chen, L. Li, Carbohydrate Polymers, 104 (2014) 1-7.

[36] S.Y. Oh, D.I. Yoo, Y. Shin, H.C. Kim, H.Y. Kim, Y.S. Chung, W.H. Park, J.H. Youk, Carbohydrate Research, 340 (2005) 2376-2391.

[37] W. Lan, C.-F. Liu, R.-C. Sun, Journal Of Agricultural And Food Chemistry, 59 (2011) 8691-8701.

[38] J. Sundberg, G. Toriz, P. Gatenholm, Cellulose, 22 (2015) 1943-1953.

[39] M. Adsul, S.K. Soni, S.K. Bhargava, V. Bansal, Biomacromolecules, 13 (2012) 2890-2895.

[40] C.-H. Kuo, C.-K. Lee, Carbohydrate Polymers, 77 (2009) 41-46.

[41] E. Lizundia, A. Urruchi, J.L. Vilas, L.M. Leon, Carbohydrate Polymers, 136 (2016) 250-258.

[42] M. Roman, W.T. Winter, Biomacromolecules, 5 (2004) 1671-1677.

[43] X. Liu, L. Yu, H. Liu, L. Chen, L. Li, Cereal Chemistry, 86 (2009) 383-385.

[44] M.D.C. Lucena, A.E.V. de Alencar, S.E. Mazzeto, S.D. Soares, Polymer Degradation And Stability, 80 (2003) 149-155.

Graphical Abstract

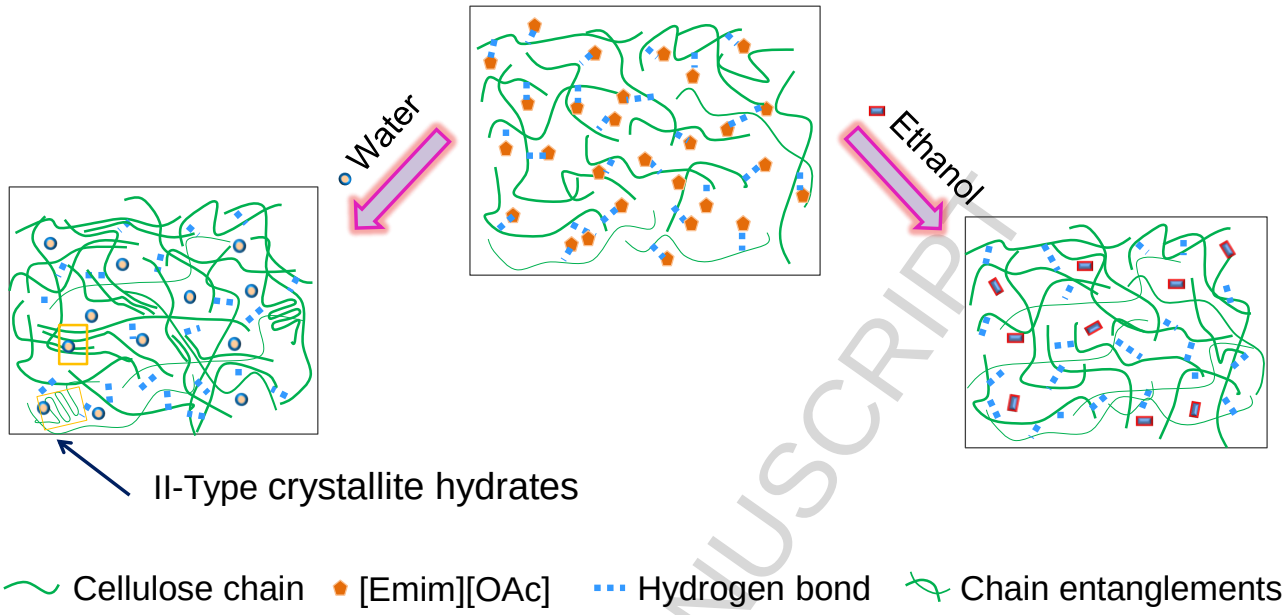

Highlights:

- ✓ The antisolvent determines the structure of regenerated cellulose
- ✓ Water promotes cellulose molecular rearrangements and structural aggregation
- ✓ Ethanol leads to regenerated cellulose with lower crystallinity than does water